Doping Highly Ordered Organic Semiconductors: Experimental Results and Fits to a Self-Consistent Model of Excitonic Processes, Doping, and Transport

Si-Guang Chen, Paul Stradins, and Brian A. Gregg*

National Renewable Energy Laboratory, 1617 Cole Boulevard, Golden, Colorado 80401

Received: February 3, 2005; In Final Form: May 23, 2005

An in-depth study of n-type doping in a crystalline perylene diimide organic semiconductor (PPEEB) reveals that electrostatic attractions between the dopant electron and its conjugate dopant cation cause the free carrier density to be much lower than the doping density. Measurements of the dark currents as a function of field, doping density, electrode spacing, and temperature are reported along with preliminary Hall-effect measurements. The activation energy of the current, E_{aJ}, decreases with increasing field and with increasing dopant density, n_d. It is the measured change in E_{aJ} with n_d that accounts primarily for the variations between PPEEB films; the two adjustable parameters employed to fit the current−voltage data proved to be almost constants, independent of n_d and temperature. The free electron density and the electron mobility are nonlinearly coupled through their shared dependences on both field and temperature. The data are fit to a modified Poole−Frenkel-like model that is shown to be valid for three important electronic processes in organic (excitonic) semiconductors: excitonic effects, doping, and transport. At room temperature, the electron mobility in PPEEB films is estimated to be 0.3 cm^2/Vs; the fitted value of the mobility for an ideal PPEEB crystal is 3.4 ± 2.7 cm^2/Vs. The modified Poole−Frenkel factor that describes the field dependence of the current is $2 \pm 1 \times 10^{-4}$ eV $(cm/V)^{1/2}$. The analytical model is surprisingly accurate for a system that would require a coupled set of nonlinear tensor equations to describe it precisely. Being based on general electrostatic considerations, our model can form the requisite foundation for treatments of more complex systems. Some analogies to adventitiously doped materials such as π-conjugated polymers are proposed.

Introduction

The study of organic semiconductors, OSCs, is a field of increasing interest, partly because of the increasing number of actual and potential applications of OSCs such as in electrophotography,[1] electroluminescent devices, flexible integrated circuits, and solar cells.[2,3] OSCs are fundamentally different than most inorganic semiconductors, ISCs, and these differences must be clearly understood before OSCs can be optimally employed in devices.[4,5] We also must distinguish between molecular OSCs[5,6] and π-conjugated polymeric OSCs.[7,8] Molecular OSCs have no covalent bonds between the individual molecules in the solid. They are almost never substantially doped because it is difficult to introduce free charge carriers into them, while, on the other hand, it is difficult *not* to dope ISCs and π-conjugated polymeric OSCs. We have discussed these differences in detail[9−12] and give here just a brief overview, considering first ISCs. Morphological defects break or distort the high-energy interatomic covalent/ionic bonds in ISCs. This, along with the relatively high dielectric constant and the spatially extended carrier wave functions, often produce electronic states in the band gap that can result in mobile charge carriers. Dopants in ISCs, which are usually substitutionally incorporated atomic species with a valence different from the host lattice, efficiently produce free carriers. These and other doping processes are so facile that only the most perfect ISC crystals approach the intrinsic (undoped) state. On the other hand, molecular OSCs are lattice-bonded only through weak van der Waals or hydrogen bonds. Breaking these low-energy bonds at morphological defects ("noncovalent disorder") does not often produce charged species. Moreover, it is not possible to introduce substitutional dopants having a different valence in molecular OSCs because all covalent bonds occur intramolecularly. Most molecular OSCs are therefore quasi-intrinsic, even in disordered or amorphous films. Doping of molecular OSCs is only now beginning to be explored in quantitative studies. Intermediate between the extremes of ISCs and molecular OSCs lie π-conjugated polymers. Bends, twists, and defects in their π-conjugated backbone ("covalent disorder") tend to generate a large number of equilibrium charge carriers,[10,11] yet only a few of them are free because $\gamma > 1$ (see Figure 1 and eq 1).

We present here what is, to our knowledge, the first comprehensive study of doping in a well-defined molecular OSC. The crystal structure of the host is known and the n-type dopants are commensurate in the host lattice, that is, they fit substitutionally in the same lattice sites as the host and do not disturb the crystal structure of the film.[11,13] The dopant is chemically a close relative of the host and the two have identical reduction potentials (electron affinities),[14] thus electrical potential wells and barriers in the films are caused only by internal Coulomb forces, not by differences in redox potentials. This system minimizes the number of unknowns and allows a more quantitative analysis of doping and transport in molecular OSCs than has yet been reported.[9] Nevertheless, there are still two important (and coupled) parameters that we cannot unambiguously separate: the free electron mobility, μ_f, and the free electron density n_f. The reasons for this, its consequences, and its relevance to other studies of OSCs are discussed in detail here and in the Appendix.

* Address correspondence to this author. E-mail: brian_gregg@nrel.gov.

10.1021/jp0506080 CCC: $30.25
Published on Web 06/28/2005

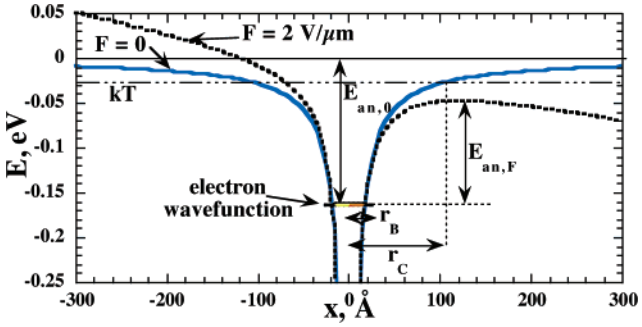

Figure 1. A schematic representation of energy levels in an excitonic semiconductor, XSC. The calculations assume Coulomb's law with the positive charge at 0 Å in an isotropic medium. The ratio of the width of the Coulomb potential well at kT, r_C, and the Bohr radius of the carrier wave function, r_B, is defined as $\gamma = r_C/r_B$ (see eq 1). Under an applied field, F, the activation energy for thermal emission of a charge carrier out of a Coulomb potential well, $E_{an,F}$, decreases with the square root of the applied field, $F^{1/2}$ (Poole−Frenkel mechanism).

The transport,[15−26] doping,[9,14,27−33] and excitonic processes[34−42] in OSCs[43] have been the subject of many studies. Most of these studies focus on a single process and use a single model to describe it. Unfortunately, these models often become self-contradictory when applied to transport *and* doping *and* excitonic processes. Existing models are usually based on the study of special systems such as undoped single crystals or molecularly "doped" polymers (i.e., insulating polymers containing dissolved electroactive small molecules—not doped in the sense of adding charge carriers). The extension of these models beyond their foundations to the descriptions of disordered molecular semiconductors, doped systems, and π-conjugated polymers is questionable. One typical problem of these models is that the Coulomb attraction between charge carriers and their conjugate counterions is ignored; another is that the equilibrium carrier density in disordered materials is neglected. Here we attempt to describe the "big picture" for the first time using a self-consistent model of the transport, doping, and excitonic processes in OSCs.

Excitonic Semiconductors

To make sense of the results presented below, we must first briefly describe the properties of excitonic semiconductors. There are two fundamental parameters that distinguish excitonic (usually organic) semiconductors, XSCs, from conventional semiconductors, CSCs (usually ISCs): the dielectric constant, ϵ, and the Bohr radius of the relevant charge carrier, r_B. As described previously[11,12] and illustrated in Figure 1, a semi-quantitative distinction between these two general types of semiconductors can be described by a function designated γ:

$$\gamma = \frac{r_c}{r_B} \approx \left(\frac{q^2}{4\pi\epsilon_0 k_B r_0 m_e}\right)\left(\frac{m_{eff}}{\epsilon^2 T}\right) \approx \frac{E_{bind}}{k_B T} \qquad (1)$$

$\gamma > 1$: excitonic semiconductor, XSC

$\gamma < 1$: conventional semiconductor, CSC

where q is the electronic charge, ϵ_0 is the permittivity of free space, k_B is Boltzmann's constant, r_0 is the first Bohr radius of an electron in a hydrogen atom, m_e is the mass of a free electron in a vacuum, m_{eff} is the effective mass of the electron in the semiconductor (usually less than m_e in CSCs but greater than m_e in XSCs), and T is the absolute temperature. There are several approximations in eq 1,[11,12] for example, the correlation energy is ignored so that the energy of an electron in an exciton is considered to be the same as that of a dopant electron near its conjugate cation. Another way to view the function γ is as the ratio of the binding energy of an electron in its lowest Bohr orbital, E_{bind}, to the thermal quantum k_BT (eq 1); thus it describes the degree of thermal ionization of electrons (or holes). When $\gamma > 1$, most carriers will be bound rather than free.

The structures of the XSC perylene diimide, PPEEB, and its n-type dopant were described previously.[9,13,14] The dopant is a reduced derivative of PPEEB containing a covalently bound positive countercharge to the "free" electron. PPEEB films form highly crystalline smectic C-like, but solid, films with the layer plane parallel to the surface. The conductivity is highest along the $\pi-\pi$ stacking axis that lies parallel to the substrate. EPR studies show that even the electrostatically "bound" electrons are substantially delocalized over ~5−10 molecules along this axis.[13,44]

Field Dependence of n_f. Figure 1 shows a schematic energy diagram of an XSC, both with and without an applied electric field, F. The average electron is localized in a Coulomb potential well near its conjugate cation (or conjugate hole in the case of an exciton) because the delocalization length of its wave function (r_B) is smaller than the width of the Coulomb well at k_BT (r_C), that is, its binding energy is greater than k_BT. It is because $\gamma > 1$ that excitons are formed in XSCs upon absorption of light, and that most added dopant electrons, independent of the redox potential of the dopant, will be bound near their conjugate cations.[12] The same phenomena occur in CSCs at cryogenic temperatures,[9,45,46] where they become XSCs (eq 1). In such cases, the density of *free* electrons, n_f, at equilibrium, as a function of the added n-type dopant density, n_d, is:

$$n_f = n_d \exp(-E_{an,0,nd}/k_BT) \qquad (2)$$

where the zero-field activation energy for free carriers, $E_{an,0,nd}$ is shown in Figure 1. Fermi−Dirac statistics here can be reduced to Boltzmann statistics because $E_{an,0} \gg k_BT$. In some idealized 2-state systems the denominator in eq 2 would be $2k_BT$;[47] however, this asssumed mechanism would also require that n_f increase as $n_d^{1/2}$. Since we have never observed such behavior under a large range of experimental conditions,[9,12,14] we feel justified in using eq 2.

In this work, we must distinguish between a number of different but related quantities. For example, there are numerous activation energies of interest. Our nomenclature employs subscripts to distinguish between them: for example, $E_{ax,F,nd}$ means the activation energy of x (where $x = J$, n_f, or μ_f, i.e., current density, free carrier density, or free carrier mobility) under conditions of variable F and n_d. Often we will be interested in the activation energy at zero field, $E_{ax,0,nd}$, or at zero doping density, $E_{ax,F,0}$. We use as few subscripts as possible, thus, E_{aJ} is the activation energy of the current under otherwise undefined conditions. Other variables are treated similarly.

Under an applied electric field, the barrier height of the potential well confining the electron decreases (Figure 1), thus increasing the free electron density, n_f. If the potential is assumed to be a Coulomb potential, the corresponding increase in J with F is described by the well-known Poole−Frenkel (PF) equation:[48]

$$J = qF\mu^0 n_d \exp((-E_{an,0,nd} + a_n F^{1/2})/k_BT) \qquad (3)$$

where μ^0 is the carrier mobility (but see eqs 4 and 7 below) and $a_n = (q^3/\pi\epsilon_0\epsilon)^{1/2} = (7.59 \times 10^{-4})/\epsilon^{1/2}$ eV (cm/V)$^{1/2}$.

Field Dependence of μ_f. The mobility of charge carriers in XSCs usually increases with increasing electric field. This

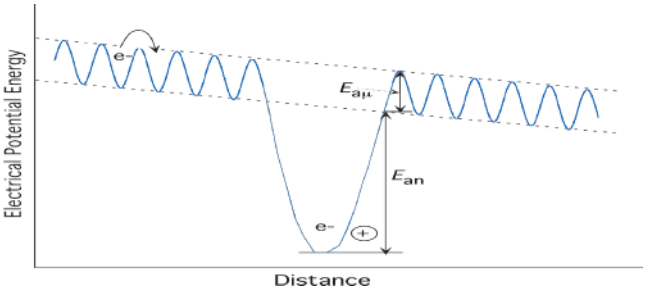

Figure 2. Schematic 1-dimensional potential energy diagram under an applied field showing the fluctuations in the conduction band that limit the mobility (effective depth = $E_{a\mu}$) and the potential well created by a dopant (effective depth = E_{an}). Both of these activation energies are affected similarly by an applied field (eqs 6 and 7). The spatial extent of the electron wave function (shown in Figure 1) is not shown here for clarity. The positive countercharge of the dopant electron is shown offset from the conducting pathway consistent with the known crystal structure of PPEEB.

process is formally independent of the field assisted increase in n_f described above. However, in practice, n_f and μ_f are coupled. Equation 3 was derived specifically to describe the increase of n_f, not μ_f, with field. However, it should be valid also for the current density of electrons surmounting a Coulomb potential *barrier* of height $E_{an,0,nd}$ (i.e., up to the point where the wave function spans the potential barrier, Figure 1 inverted). The PF model thus has obvious implications for the free carrier *mobility*, as well as the free carrier *density*. The $F^{1/2}$ term is only valid for Coulomb potentials. Other shapes of potential wells/barriers result in more complex forms of eq 3. Field-dependent mobilities are most unambiguously observed in materials that have very low values of n_f (e.g., $<10^{14}$ cm^3) such as molecularly doped polymers.[15,16] Models of charge transport in such XSCs explain the field dependence of the carrier mobility by assuming a Gaussian distribution of hopping site energies[15,16] and/or by assuming a random distribution of *fixed* dipoles in the film (a correlated medium).[18,20,49] These mechanisms have also been applied to the description of conduction in π-conjugated polymers.[18,19,22,23] We pointed out recently that a distribution of dipoles that can slowly orient in any direction should also result in a similar mechanism for the field-dependent mobility.[10] It is important to understand that the orientations of the dipoles in doped PPEEB are free to change with changing internal electric fields: they are *not* randomly oriented *fixed* dipoles. This is also expected to be true in most doped (purposely or not) organic materials.

A mobility for free carriers of the empirical form[7,19,20]

$$\mu_f = \mu^0(T)\exp(\alpha(T)F^{1/2}) \tag{4}$$

is often employed where the T-dependences of μ^0 and α are unknown; μ^0 is here the mobility when $\alpha = 0$, that is, when μ is independent of field. Consistent with our discussion above, we suggest that the field dependence of the mobility should have a form similar to the field dependence of the free carrier density if they are both controlled by the same factors, namely electrostatic forces. In this view, fluctuations in the conduction and valence band energies tend to localize charge carriers and make their transport thermally activated (Figure 2). That is, carriers must be thermally emitted out of traps or over barriers to contribute to the current. Assuming as above that both traps and barriers can be described as Coulomb potentials, we rewrite eq 4 as

$$\mu_f = \mu^0(T)\exp((-E_{a\mu,0,nd} + a_\mu F^{1/2})/k_BT) \tag{5}$$

where $E_{a\mu,0,nd}$ is the zero-field activation energy for the mobility at n_d, and a_μ corresponds to a_n in eq 3 and describes the field dependence of the mobility. Although a_n has an expected value (eq 3), a_μ is not known. We expect it to be similar in magnitude, but less than, a_n because mobile carriers can avoid some of the traps and move around many of the barriers that hinder their motion.

The assumed functional form for the variation in μ_f with F in eq 4 is quite similar to, and in eq 5 is identical to, the variation in n_f with F in the PF mechanism. Conceptually therefore, eq 3 could be describing the change in J caused by the increase in either n_f or μ_f with $\exp(F^{1/2})$. In fact, eq 3 is describing both and there is often no simple way to distinguish between them (Figure 2), especially in doped XSCs (see the Appendix). Many studies overlook the increase in n_f with $\exp(F^{1/2})$ and attribute the observed behavior entirely to the increase in μ_f with $\exp(F^{1/2})$. Except for studies of single crystals and molecularly doped polymers, this approach seems to lack theoretical justification.

Electrostatic dipoles resulting from any compensated charges in the material, including those caused by purposely added dopants, create one trap and one barrier. On a two- or three-dimensional energy surface (but not in 1-D, as in Figure 2), localized traps are more influential than localized barriers, because barriers tend to repel carriers, and thus carriers often go around them rather than over them. Traps attract carriers, however, forcing the carriers to then be emitted from the traps (note that traps are not recombination sites in PPEEB, and in many XSCs, because there are essentially no minority carriers with which to recombine). Grain boundary barriers, however, are not localized and thus are unavoidable for carriers that must pass through multiple crystallites. Crystallite grain boundaries may be "vertical" (i.e., abrupt) barriers rather than the Coulomb barriers treated in the (inverted) PF mechanism.

Coupling between n_f and μ_f. The internal electric field in a device is affected by both n_f and μ_f. Therefore, n_f and μ_f are coupled to each other through the internal electric field.[50] This is a nonlinear effect that cannot be adequately described by analytical equations.[51] For this reason and others, we cannot know a priori the expected prefactor to the F dependence for either n_f or μ_f (i.e., the magnitudes of a_n or a_μ in eqs 3 and 5, respectively). Since our experiments cannot distinguish between a_n and a_μ, and they should be coupled, we define

$$\eta = (a_n + a_\mu - \text{coupling factor}) \tag{6}$$

There are other possible reasons to replace the PF factors, a_n and a_μ, with η. For example, our equations neglect the anisotropy of the dielectric constant and the current, assume only Coulomb potentials, etc., thus we cannot expect the PF factors to be exact. Equation 6 is an attempt at a reasonable analytical approximation to a nonlinear process. Ultimately therefore, we employ eq 7 (similar to eq 3 except for the definition of some terms) to fit the experimental $J-F$ curves:

$$J = qF\mu^0 n_d \exp((-E_{aJ,0,nd} + \eta F^{1/2})/k_BT) \tag{7}$$

where μ^0, as in eqs 4 and 5, represents the "pristine" single-crystal mobility of free carriers unperturbed by dopants, traps, electrostatic fluctuations, etc. We show below that μ^0 is independent of n_d, F, and T, within experimental error, and that eq 7 is an excellent fit to our $J-F-T$ data.

In the temperature-dependent measurements, we must account for the coupling between n_f and μ_f in the single kinetic step of current production ($J = qF\mu_f n_f$). The sum of their individual

activation energies, $E_{an} + E_{a\mu}$, appears as the experimentally measurable E_{aJ} of the current (Figure 2). We have no exact method of distinguishing between E_{an} and $E_{a\mu}$, although we can obtain approximate values. This is a common problem in measurements of OSCs. In some cases one can measure μ_f independent of n_f, or vice versa; however, this is quite difficult in *doped* OSCs as discussed in the Appendix.

Experimental Section

The dopant and PPEEB were synthesized as described previously.[14,52,53] Solutions of these two compounds were prepared in a nitrogen atmosphere glovebox. The PPEEB films are doped by adding aliquots of the dopant solution to the solution of PPEEB. Solid films of PPEEB undergo a spontaneous transition from a red to a black phase;[52,53] all measurements were performed in the thermodynamically stable black phase.

Conductivity was measured on Pt interdigitated electrodes (IDEs); the film thickness was approximately equal to the electrode height of 110 nm. Some of the IDEs were purchased from AbTech (abtechsci.com) and some were produced in-house. The in-house IDEs consisted of six electrode patterns having electrode spacings of 3.6, 6.8, 12.2, 26, 52, and 102 μm. All had an electrode area of 10^{-4} cm^2 and a total electrode length of 10 cm. Doped PPEEB films were spin-coated onto the IDEs.

We employed a Keithley 236 Source-Measure Unit for the $I-V$ measurements which were controlled by a program written in LabVIEW 6. Samples were mounted in a Hansen Vacuum Shroud Cryostat and their temperature was controlled by a Lake Shore temperature controller. Samples were mounted into the cryostat in an inert atmosphere glovebox. The cryostat was then sealed, transferred to laboratory ambient, and evacuated by a Pfeiffer turbomolecular pump. Conductivity measurements confirmed that samples were not contaminated by oxygen while in the cryostat. Temperature-dependent $I-V$ measurements commenced at 150 K and increased in 30 K increments to room temperature. The temperature was first allowed to equilibrate for 10−15 min at each T setpoint. In the subsequent $I-V$ scan, the delay time was set to 2 s or longer, depending on T, to ensure current reproducibility at each voltage value. Measurements at 3−6 different electrode spacings were made at each temperature. From $I-V$ curves, current density−average field, $J-F$, curves were obtained.

The Hall effect measurements were performed with a Bio-Rad HL5500 Hall effect measurement system. The sample was patterned in a symmetrical cross geometry (arm length ca. 3 mm, width ca. 1 mm) with electrical contacts to the four extrema of the cross. The Seebeck effect measurements were performed with a system built in-house described previously.[54]

Results

Electrode Spacing Dependence of the Current. A number of measurements were made of current density, J, in the doped PPEEB films as a function of field, F, dopant density, n_d, temperature, T, and electrode spacing, d. Typical $J-F$ dependences for a 4.8×10^{17} cm^{-3}-doped film are shown in Figure 4 at two electrode spacings of $d = 3.6$ and 26 μm. The smallest electrode spacing, $d = 3.6$ μm, is slightly smaller than the average crystallite diameter in PPEEB films, ~5−10 μm. Therefore, at $d = 3.6$ μm, some of the crystallites spanned the electrode spacing giving quasi-single-crystal behavior. The data show a quasi-ohmic (linear) regime at low field transitioning to a superlinear regime at higher field. The apparent decrease in J with d seen in Figure 3 is not always observed. Over about

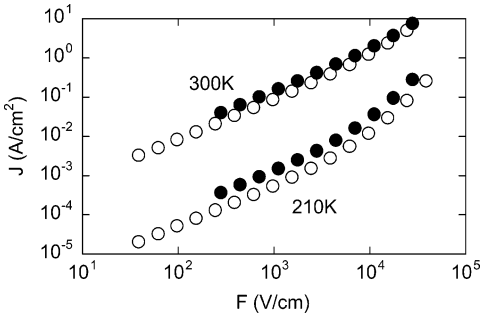

Figure 3. Electrode spacing dependence of $J-F$ curves at two different temperatures for $n_d = 4.8 \times 10^{17}$ cm^{-3}. Solid circles, $d = 3.6$ μm spacing; open circles, $d = 26$ μm spacing.

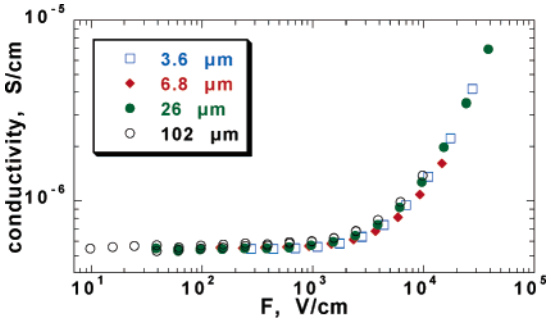

Figure 4. Electric field dependence of the conductivity of a 4.8×10^{17} cm^{-3}-doped sample for four different electrode spacings. Conductivities are normalized at their low field values.

40 samples studied, we observed no consistent spacing dependence of J. We believe that the relatively small variations of J with electrode spacing are largely caused by sample inhomogeneity, resulting in slight variations of film thickness, carrier mobility, and other film parameters. These results show that neither crystallite boundaries nor contact interfaces strongly affect the $J-F$ behavior. We note that our films are spin-coated onto preexisting contacts, thus they are not damaged or chemically altered by the evaporation of contacts such as occurs in many studies of XSCs.[55]

We further investigate whether the superlinear region seen in Figure 3 is caused by the electric field alone or is a result of space-charge-limited currents (SCLC, see also the Appendix). The lack of distance dependence of the current (Figure 3) argues against SCLC. To further support this conclusion, we plot the conductivity, $\sigma = J/F$, as a function of field for four different electrode spacings in Figure 4. The low-field conductivities varied by about a factor of 3 for different electrode spacings. These variations are random and are not related to SCLC, and thus the conductivities were normalized at their low-field values.

The data for all four spacings (Figure 4) from 3.6 to 102 μm form a single σ vs J curve. Thus the increase in conductivity at high F is a function of electric field only and is not affected by the electrode spacing. Space-charge-limited currents, on the other hand, would give an apparent conductivity

$$\sigma = J_{SCLC}/F = 9\epsilon\epsilon_0\mu F/8d \qquad (8)$$

which is inversely proportional to the electrode spacing. This d-dependence holds also in the trap-limited SCLC case. Our coplanar geometry might yield a slightly different result than eq 8, that was derived for a sandwich configuration, yet one expects a similar d-dependence of σ for SCLC. Because of the lack of any noticeable dependence of σ on d when the latter varies by a factor of 28, we conclude that the field-dependent increase in σ is not caused by SCLC.

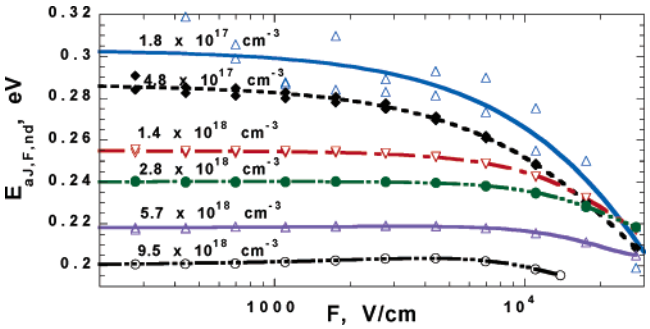

Figure 5. Activation energy for the current, $E_{aJ,F,nd}$, as a function of field, F, and doping density, n_d. The curves are third-order polynomial fits that have no theoretical significance.

Moreover, we see no evidence that the measured currents are injection limited at the contacts.[55] If they were, the applied voltage would drop mainly near the contacts rather than across the bulk sample. This is most likely to occur under conditions of low applied voltage, small electrode spacing, and low doping density. Yet over a voltage range from 10 mV to 110 V, electrode spacing from 3.6 to 102 μm, and doping density from 10^{16} to 10^{19} cm^{-3}, we observe no qualitative change in the $J-F$ behavior, and thus no evidence for injection limitations. Therefore, we further consider our results in the framework of the modified Poole−Frenkel mechanism (eq 7) and concentrate on a single electrode spacing of $d = 3.6$ μm.

Activation Energies for Current. As explained above, we expect the activation energies for the current to decrease at high fields because of the PF effect. The activation energies for a doping series were measured over a range of applied field at $d = 3.6$ μm as shown in Figure 5.

Three observations can be made from this figure. First, the monotonic decrease of $E_{aJ,F,nd}$ with F at moderate doping density ($<10^{18}$ cm^{-3}) is as expected from the PF mechanism. Second, the zero field activation energies decrease with increasing doping density as we predicted earlier and explained as a consequence of the increasing dielectric constant with n_d.[9] Third, as the doping density increases, there is a pronounced flattening of the E_{aJ} vs F curve at low F until at $n_d = 1$ mol % ($=9.5 \times 10^{18}$ cm^{-3}), E_{aJ} actually slightly *increases* at low F. The regularity of the latter trend gives it credence beyond the experimental fluctuations. This behavior at high n_d is too complex to be described by the PF mechanism alone. Similar behavior has been observed previously by Borsenberger et al. in molecularly doped amorphous polymers.[56]

We previously fit the room-temperature conductivity vs n_d data to:[9]

$$\sigma = q\mu_n n_d \exp\{(-E_{aJ,0,0} + \beta n_d^{1/3})/k_B T\} \qquad (9)$$

where β was a fitting parameter that accounted for the increase in effective dielectric constant with average distance ($n_d^{-1/3}$) between dopants, and μ_n was the room-temperature mobility averaged over doping density. The fitted value obtained from these previous studies at room temperature was $\beta = 6.5 \times 10^{-8}$ eV cm. It is because the electrons from the dopant molecules are free to orient in almost any direction with respect to their bound cations (consistent with the low dimensionality of the crystal) that adding dopants increases the effective dielectric constant. If the dopant dipoles were fixed but randomly oriented, a different treatment would be required. An alternative, perhaps parallel, possibility is the effect of the internal fields produced by the dopants. These fields originate both from cation−electron dipoles and from individual stationary charges, as some

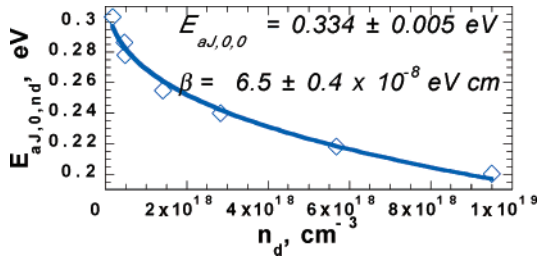

Figure 6. The extrapolated zero-field activation energies plotted versus doping density. The fit is to eq 10.

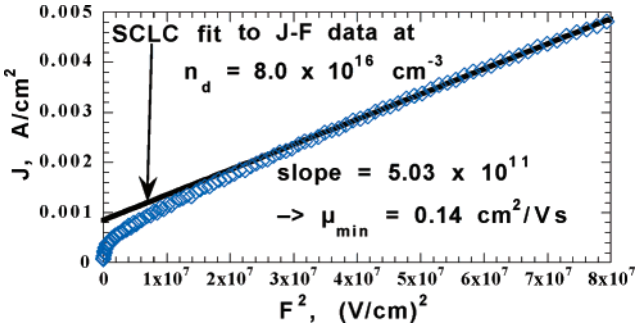

Figure 7. Average $J-F$ data from two low-doped films in both polarities fit to the space-charge-limited current model. This model provides a lower limit to the actual mobility.

compensation effect is likely to occur. These internal electric fields can lower the activation energies for dopant electrons via the Poole−Frenkel mechanism just as an external field does. Both the above effects (orientational polarization and internal fields) are expected to lower the activation energy at zero field and make it less field dependent with increasing doping density.

The new data on activation energies versus n_d (Figure 5) provide an independent method of measuring β. Considering eq 9, the zero-field activation energy is:

$$E_{aJ,0,nd} = E_{aJ,0,0} - \beta n_d^{1/3} \qquad (10)$$

The experimental zero-field activation energies, $E_{aJ,0,nd}$, are obtained from the intercepts of the polynomial fits in Figure 5. These are plotted against n_d and fit to eq 10 (Figure 6) with the following fit parameters: $E_{aJ,0,0} = 0.334 \pm 0.005$ eV, $\beta = 6.5 \pm 0.4 \times 10^{-8}$ eV cm. Obtaining an identical value of β from two independent sets of measurements lends confidence to the analysis.

Estimating the Activation Energies for Carrier Density and Mobility. It is not possible in our experiments to clearly separate E_{an} from $E_{a\mu}$, as described before. Only their sum, E_{aJ}, is directly accessible (Figure 6). However, we can approximate E_{an} and $E_{a\mu}$ by several methods, one of which is illustrated here. This approximation is later shown to be consistent with all other parameters derived from our results. Figure 7 shows the current density data at room temperature for two low-doped films ($n_d = 8.0 \times 10^{16}$ cm^{-3}) plotted versus the square of the field. The figure contains the average of four sets of data (two films in both polarities). On this type of plot, space-charge-limited currents yield a straight line above some value of F^2.[43] Although we show below (and above) that these are not actually SCL currents, the analysis is still useful.[10] Since J is not, in fact, SCLC, the true mobility must be higher than that estimated by the SCLC model (see Appendix). Moreover, we expect the mobility to increase with decreasing doping density, as it does in most semiconductors, so the mobility at $F = 0$ and $n_d = 0$, $\mu_{0,0}$, must be higher than that estimated from Figure 7. The

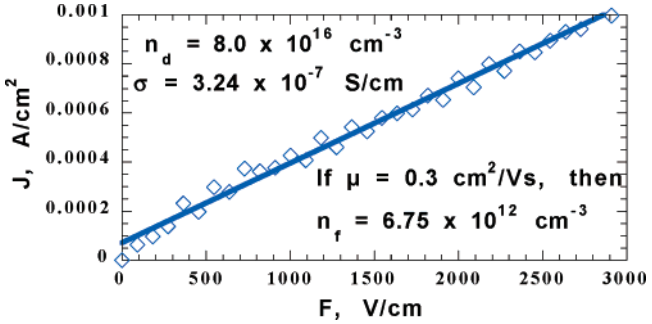

Figure 8. $J-F$ data from the low-doped films of Figure 7 in the low-field region fit to $J = q\mu_{0,0}n_fF$.

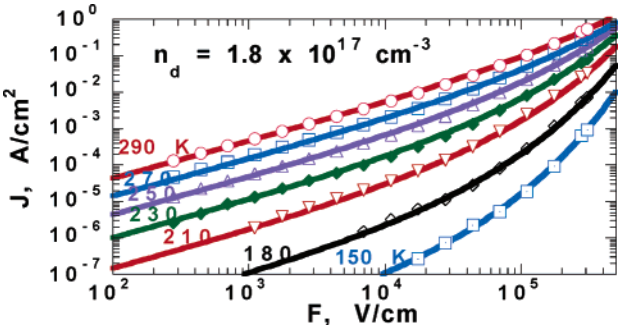

Figure 9. Current density−average field curves at various temperatures for a film doped at 1.8×10^{17} cm^{-3} with an electrode spacing of 3.6 μm. Fits are to eq 7.

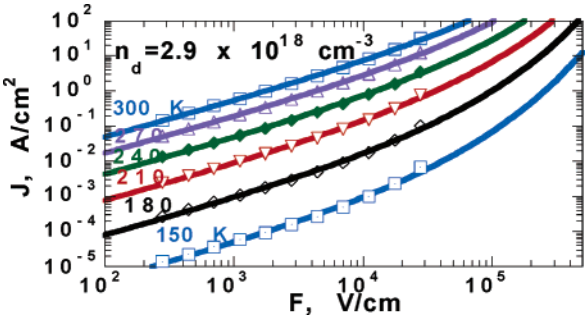

Figure 10. Current density−average field curves at various temperatures for a film doped at 2.9×10^{18} cm^{-3} with an electrode spacing of 3.6 μm. Fits are to eq 7.

mobility derived from the SCLC fit to the data in Figure 7 is $\mu_{min} = 0.14$ cm^2/Vs. The mobility averaged over all doping densities calculated previously[9] was $\mu_{avg} = 0.20$ cm^2/Vs. The Hall effect measurements (see Appendix) suggest $\mu_{Hall} \approx 0.5$ cm^2/Vs (with substantial uncertainty). All of these are room-temperature measurements. We therefore *assume* that $\mu_{0,0} = 0.3$ cm^2/Vs. This value is probably correct to within ±50%. Note that none of the major conclusions in this paper depend on this assumption; it is employed only to provide an estimate of $E_{an}/E_{a\mu}$.

This approximate value of $\mu_{0,0}$ can now be employed to estimate the zero field free charge carrier density, n_f, derived from the linear portion of the $J-F$ curve of the same films by $J = q\mu_{0,0}n_fF$. This is shown in Figure 8.

By using Boltzmann statistics, $E_{an,0,nd}$ can now be calculated from $n_f = n_d \exp(-E_{an,0,nd}/kT)$ with $n_d = 8.0 \times 10^{16}$ cm^{-3} and $n_f = 6.75 \times 10^{12}$ cm^{-3} leading to $E_{an} \approx 0.243$ eV. From the fit in Figure 6, the value of E_{an} at zero n_d can be extrapolated from $E_{an,0,0} = E_{an} + \beta n_d^{1/3}$ resulting in $E_{an,0,0} \approx 0.271$ eV for carrier density. Therefore, $E_{a\mu,0,0} \approx 0.334 - 0.271 \approx 0.063$ eV is the approximate activation energy for the mobility. Similar numerical values can be estimated via simple electrostatic calculations.[9,57] Many of the values estimated or measured in this work, along with their physical descriptions, are collected in Table 1.

***J−F−T* Data.** The $J-F$ curves of approximately 40 films with varying n_d and d were measured, most of them at multiple temperatures, and fit to eq 7. There are two fitting parameters per $J-F$ curve: μ^0 and η. Representative $J-F-T$ data for two of the films and their fits to eq 7 are shown below (Figures 9 and 10). Results from a low-doping concentration, $n_d = 1.8 \times 10^{17}$ cm^{-3}, are shown in Figure 9. This value of n_d corresponds to $E_{aJ,0,nd} = 0.303$ eV (Figure 6).

Figure 10 shows $J-F$ curves at a doping density of 2.9×10^{18} cm^{-3}. In this case, $E_{aJ,0,nd} = 0.240$ eV.

The two-parameter fits to eq 7 of all the $J-F-T$ data were excellent. The values of μ^0 obtained from the fits were independent of T within experimental error. The variation of μ^0 as a function of n_d was (as expected) random within experimental error. The average μ^0 obtained from the films was 3.4 ± 2.7 cm^2/Vs (Table 1). Given the above estimate of $E_{a\mu,0,0} \approx 63$ meV, this value of μ^0 is compatible with the estimated value of $\mu_f \approx \mu^0 \exp(-E_{a\mu,0,nd}/k_BT) = 0.30$ cm^2/Vs at room temperature. This self-consistency lends additional support to the estimated value of $E_{an,0,0} = E_{aJ,0,0} - E_{a\mu,0,0}$ (Table 1).

The values of η, the modified Poole−Frenkel prefactor (eq 6), obtained from the fits to eq 7 were also, within the rather large experimental error, independent of n_d. However, they appeared to monotonically decrease with T.

Discussion

Electronic processes in excitonic semiconductors (XSCs, defined in eq 1) are usually controlled by Coulomb forces because $\gamma > 1$. For example, these processes may be governed by electrostatic interactions between the following: (1) the incipient electron and hole of an exciton; (2) the electron of an n-type dopant and its lattice-bound conjugate cation; (3) a defect-induced hole in a π-conjugated polymer and its relatively more

TABLE 1: Estimated or Measured Values and Their Physical Descriptions

symbol	value	description
$E_{aJ,0,0}$	0.334 ± 0.005 eV	fitted activation energy for current at $F = 0$ and $n_d = 0$ (eq 10 and Figure 6)
$E_{an,0,0}$	0.271 eV	estimated activation energy of free carriers at $F = 0$ and $n_d = 0$
$E_{a\mu,0,0}$	0.063 eV	estimated activation energy for mobility at $F = 0$ and $n_d = 0$
β	$(6.5 \pm 0.4) \times 10^{-8}$ eV cm	fitted parameter describing the change in activation energy, or dielectric constant, with n_d (eq 9 and Figure 6)
$\mu_{0,0}$	0.3 cm^2/Vs	estimated electron mobility at $F = 0$ and $n_d = 0$
μ^0	3.4 ± 2.7 cm^2/Vs	fitted value of "single crystal" electron mobility (eq 7)
η	$(2 \pm 1) \times 10^{-4}$ eV (cm/V)$^{1/2}$	fitted value of the modified Poole−Frenkel factor (field dependence of the current) (eqs 6 and 7)
a_n	4×10^{-4} eV (cm/V)$^{1/2}$	approximate expected value of the Poole−Frenkel factor for charge carriers, simplest case (eq 3)
a_μ	not known	parameter determining F-dependence of μ_f, (eq 5)

tightly bound countercharge; and (4) a "free" charge carrier and the potential fluctuations it must traverse to reach the electrode, etc. In contrast, in conventional semiconductors (CSCs) these electrostatic effects are usually negligible because $\gamma < 1$. In this work we endeavor to understand and describe some of these electrostatic effects that so sharply distinguish XSCs from CSCs. Our chosen system for these studies is a polycrystalline film of liquid crystalline semiconductor in its solid phase doped with a lattice-commensurate n-type dopant. Although this may be the simplest doped XSC studied, it is still complex and not wholly understood. The major impediment to a greater understanding is our inability to clearly distinguish experimentally between the free carrier density, n_f, and the free carrier mobility, μ_f (see also the Appendix).

The fundamental influence of the electrostatic forces in XSCs is not limited to the purposely doped materials described here. All semiconductors have charged species in them and when $\gamma > 1$, electrostatic forces between these charges control much of their electrical behavior. The equilibrium free carrier density in XSCs increases with increasing disorder just as it does in CSCs. But there are two qualitatively distinct types of disorder in XSCs: the *noncovalent disorder* occurring in molecular semiconductors where only weak intermolecular van der Waals and hydrogen bonds are bent or broken, and the *covalent disorder* occurring in π-conjugated polymers in which strong interatomic conjugated bonds are bent and broken. The equilibrium free carrier density increases with increasing bond strength of the compromised bonds. In other words, breaking or distorting weak bonds generates electronic states near the band edges, while breaking or distorting strong bonds can generate states deep in the band gap. Therefore, the adventitious carrier density, n_a, is usually highest in amorphous materials with covalent disorder such as π-conjugated polymer films, while n_a is lower in amorphous molecular OSCs, and lowest in crystalline molecular OSCs. A fraction of n_a will generate free carriers, n_f, by the same mechanisms discussed above for purposely added dopants, n_d. The concentration of these free carriers will be affected by field, temperature, dielectric constant, etc. in an identical fashion to the purposely added dopants. Being based on fundamental and unavoidable electrostatic considerations, our analysis is quite general; it applies to a much broader range of material systems than just the doped PPEEB films described here. It may form the requisite foundation for treatments of more complex systems, such as those disordered materials with densities of states (DOS) that tail off into the band gap.

Some numerical examples may help illustrate the importance of adventitious doping in XSCs.[10,44] In an undoped (intrinsic) semiconductor, the intrinsic free electron density is calculated from basic thermodynamics as

$$n_i = N_c \exp(-E_{BG}/2k_BT) \tag{11}$$

where N_c is the density of conduction band states and E_{BG} is the band gap energy. If we take a typical XSC band gap of 2.0 eV and $N_c = 10^{20}$ cm^{-3}, the intrinsic carrier density is $n_i \approx 2 \times 10^3$ cm^{-3}. This is an immeasurably small number. The *actual* free carrier density, n_f, in an XSC can be estimated by measuring the dark conductivity extrapolated to zero field and the zero field carrier mobility: $n_f = \sigma/q\mu_n$. Even in the highly purified, undoped polycrystalline PPEEB films, this procedure leads to $n_f \approx 10^9$ cm^{-3}. That is, n_f is 6 orders of magnitude greater than n_i. This is caused by chemical and physical defects in the film. In π-conjugated polymers (*covalently* disordered systems) such as PPV derivatives, this procedure leads to $n_f \approx 10^{17}$ cm^{-3}, according to extrapolated data and directly reported results.[8,25,26,44,58] The total adventitious charge density, n_a, is probably 2−3 orders of magnitude greater than the free carrier density, n_f, because $\gamma > 1$. This suggests that the average distance between charges is 5−10 nm in PPV derivatives, which may explain why the exciton diffusion length is on this order. Measurement of the spin density in "undoped" polyacetylene shows a spin concentration of 10^{18} cm^{-3};[43] this represents a lower limit to the carrier density since it does not include the spinless carriers. In short, there is a huge increase (5−9 orders of magnitude) in total charge density between materials with only noncovalent disorder such as PPEEB and materials with both covalent and noncovalent disorder such as π-conjugated polymers. In both classes of materials, the intrinsic carrier densities are negligible compared to $n_d + n_a$. Most existing treatments of XSCs ignore the adventitious doping density, n_a, make no distinction between covalent and noncovalent disorder, and neglect the fact that n_f is a strong function of F (and T, n_d, ϵ, etc.). These are serious omissions. Moreover, the theoretical treatment of transport in XSCs is usually based on models with these omissions plus the assumption of *randomly oriented, fixed dipoles* in the semiconductor film. This assumption does not seem physically realistic[59] except in cases such as molecularly doped insulating polymers where n_a is very low. In most not-purposely doped XSCs, where n_a cannot be neglected, the major dipoles are caused by deeply trapped charges coupled to more weakly bound oppositely charged carriers. Such dipoles are usually *randomly positioned but free to orient* in almost any direction to minimize the free energy (at equilibrium) or the entropy production (away from equilibrium). This analysis follows directly from the results presented here and their extrapolation to other, less-well-ordered XSCs.

Our analysis of transport is somewhat different than existing models of transport that mainly treat amorphous materials. There are several reasons for this besides the obvious differences between crystalline and amorphous materials: (1) Our model is compatible with *three* processes occurring in XSCs—excitonic processes, doping and transport—whereas most existing models treat transport only. The latter models may lead to self-contradictions when applied to excitonic processes or doping. (2) Different definitions are employed for mobility and carrier density: the models for disordered systems often employ the *effective* mobility, that is, the mobility averaged over all carriers, both trapped and free. Our model treats the mobility of free carriers, μ_f, only and considers that carriers in traps are immobile. Likewise, the former models usually consider only the total carrier density whereas we distinguish between trapped carriers and free carriers, n_f. (3) We explicitly treat the electrostatic attractions between carriers and their conjugate counterions because only in this way can transport models be made compatible with doping effects and excitonic processes. Our analysis is based on the universal laws of electrostatics that underlie the observed behavior of *all* XSCs. However, the experimental behavior of an individual system can be perturbed by many factors. For example, the properties of amorphous polymers are strongly affected by the large density of intragap states. This cannot alter the fundamental electrostatic considerations described in our model, but it can cause additional complexity. Some existing models seem to focus on the additional complexity but overlook the underlying electrostatics.

Activation energies for the current densities, E_{aJ}, show the decrease in E_{aJ} with field expected from the Poole−Frenkel mechanism at low n_d. At higher n_d, however, E_{aJ} actually *increases* with F at first before eventually decreasing (Figure

5). This behavior has been observed and described by Borsenberger et al. in amorphous molecularly doped polymers studied by time-of-flight mobility measurements.[56] These authors proposed the following mechanism: At low F, carriers can move around potential barriers that hinder their transport, but increasing F forces carriers up against the barriers and makes it energetically difficult for them to move back against the field in order to go around the barriers. This causes $E_{a\mu}$ to increase with F. At still higher F, the decrease in barrier height by an inverted PF-like mechanism eventually leads to a decreasing $E_{a\mu}$. There is apparently no analytical way to describe this behavior, but Borsenberger et al. could approximate it by Monte Carlo simulations.[56] It is interesting that this behavior, observed first in amorphous XSCs, is also observed in our highly ordered system. This suggests that the phenomenon may be more general than at first realized. In the system of Borsenberger et al., the "dopant" density (uncharged but polarizable molecules that may have static dipoles) was not varied; it remained at ~50 mol %. In our system, however, the dopant (charge) density was varied over 2−3 orders of magnitude but only up to 1 mol %. Since our dopants contain actual separated charges they create much larger dipoles (electrostatic traps and barriers) than the uncharged molecular "dopants". We observe the effect of these added dipoles in increasing the activation energy, presumably for the mobility, $E_{a\mu}$, at quite low n_d (~0.1 mol % $\approx 9 \times 10^{17}$ cm^{-3}). The lower effective dimensionality of our highly ordered PPEEB system may accentuate this effect at lower dopant density compared to the amorphous system studied by Borsenberger et al.

It is not possible to cleanly separate the effects of n_f and μ_f in our experiments, as detailed above and in the Appendix. At zero field, however, we can approximate the relative importance of E_{an} and $E_{a\mu}$ as discussed above: $E_{an,0} \approx 4\, E_{a\mu,0}$, that is, most of the activation energy is related to carrier production from dopants (Figure 2). This seems reasonable since dopant electrons reside, for the most part, in relatively deep Coulomb potential wells resulting from the covalently bound cations on the side chains of the dopants, while the mobilty of the free electrons should be mainly affected by the dipoles created by the *bound* dopant electron−cation pairs, by the grain boundaries between crystallites, and by other morphological or electrical defects. Future efforts at Hall effect measurements may allow us to unambiguously separate the effects of n_f and μ_f.

The $J-F-T$ measurements over a large range of doping density, temperature, and electrode spacing were uniformly well fit by eq 7 with two adjustable parameters, μ^0 and η, both of which turned out to be constants for all films within experimental error. The fits to eq 7 also required the values of $E_{aJ,0,nd}$ that were obtained from the measurements shown in Figures 5 and 6. It is this change in $E_{aJ,0,nd}$ with n_d that accounts primarily for the variations between films. Like any analytical equation, eq 7 cannot accurately account for the nonlinear coupling between μ_f, n_f, and F. It also relies on the dubious assumptions that all potential barriers and potential wells can be treated as Coulomb potentials, and that the impediments to the mobility can be treated identically to the impediments to free carrier production. The unexpected success of eq 7 suggests that the aggregate phenomena involved in current production in XSCs may be described more simply than the consideration of each individual process would lead one to expect. As in the historical development of models describing ISCs, such approximations, if validated by further studies, may provide a useful analytical description of electronic processes in XSCs despite the fact that an exact model would require numerical simulations.

Although excellent fits to eq 7 are obtained from all of the $J-F-T$ data with two fitting parameters, the error in each of the two parameters is quite large. The apparent reason is that the fitted values of μ^0 and η are not independent: changes in one strongly affect the other.

Fitting the $J-F$ curves of multiple films to eq 7 as a function of temperature leads to the unexpected conclusion that μ^0 does not change by more than a factor of 2 or 3 throughout the 150° temperature range and throughout the dopant density range of $n_d = 10^{17}-10^{19}$ cm^{-3} of our studies. As defined in eq 7, μ^0 is a fundamental material parameter; it is the mobility in a single crystal devoid of dopants, traps, grain boundaries, and potential fluctuations. It is further assumed that μ^0 is independent of F. In such a material, $E_{aJ} = \eta = 0$. Ideally, μ^0 should be independent of n_d (as it is in our experiments). Its expected temperature dependence, however, depends on the degree of delocalization of the electrons. The two extreme cases are well-known. If electrons are delocalized, higher temperature decreases μ^0 because of increased scattering from phonons. On the other hand, if electrons are localized and must hop from site to site, higher temperature increases the hopping rate and thus μ^0. Polycrystalline perylene diimide films are known to have partially delocalized carriers[44] and excitons[42] and are thus a case intermediate between the two extremes. The temperature dependence of μ^0 in this system cannot be predicted a priori. Our results show that it is quite small, within experimental error of zero over the 150° range of our experiments.

The modified Poole−Frenkel coefficient, η, decreases slightly with temperature. This decrease is monotonic with T in all samples but still within experimental error. The value of $\eta = (2 \pm 1) \times 10^{-4}$ eV $(cm/V)^{1/2}$, being approximately half the expected Poole−Frenkel coefficient, sugggests that the coupling between n_f and μ_f (eq 6) may be similar in magnitude to η. The lower than expected value of η also might be explained by geometrical constraints: the dopant electron is actually not located in a symmetric potential well around the cation as depicted in Figure 1, but is rather in a potential well in a highly anisotropic crystal.

There is no unambiguous dependence of the $J-F$ behavior on electrode spacing. Clearly therefore, these currents are not SCLC even at the lowest doping concentration (see also the Appendix)[10,11] and their behavior approaches the lack of d-dependence expected for PF currents.

Summary and Conclusions

Electrical measurements are performed on a number of films consisting of the liquid crystalline semiconductor PPEEB doped n-type with varying amounts of its lattice-commensurate dopant. The results are interpreted with a self-consistent modified Poole−Frenkel-like model that seems to be approximately valid for all electrical processes in XSCs. Existing models of XSCs treat excitonic processes *or* doping *or* transport. None of these models, to our knowledge, is adequate when applied to excitonic processes *and* doping *and* transport. The need for a self-consistent model is clear. Our approach is based on recognizing the dominant influence of electrostatic forces on the behavior of what we have defined as excitonic semiconductors, XSCs. The electrostatic forces between charges and the spatial extent of the wave functions in XSCs determine (1) the exciton binding energy, (2) the free carrier density, (3) the change in free carrier density with applied field, (4) the doping efficiency, (5) the charge carrier mobility and its increase with applied field, and (6) the exciton mobility. In short, γ (defined in eq 1) controls the electrical characteristics of XSCs.

Our measurements show that the free carrier density, n_f, is much less than the added dopant density, n_d, and that n_f increases with increasing dielectric constant, temperature, and field. Most existing models of XSCs completely neglect n_f, despite the fact that it can dominate the electrical behavior. We expect that μ_f is nonlinearly coupled to n_f, and this is consistent with all results. Thus separating the two only by $J-F$ measurements may not be possible. They may be individually measurable under particularly favorable circumstances, but often, as in our system, one can only measure the $n_f\mu_f$ product. Accounting for the coupling between n_f and μ_f leads to a modified form of the Poole−Frenkel equation. This gives excellent fits to all of our $J-F-T$ data with two fitting parameters: the "single crystal" mobility, μ^0, and the parameter describing the modified Poole−Frenkel field dependence of the current, η. Over the range of our studies, $\mu^0 = 3.4 \pm 2.7$ cm^2/Vs and $\eta = 2 \pm 1 \times 10^{-4}$ eV (cm/V)$^{1/2}$. Both of these parameters are independent of n_d and T within experimental error.

Our analysis is based on fundamental electrostatic considerations. It should apply to amorphous molecular and polymeric excitonic semiconductors as well as to the highly ordered, substitutionally doped films described here.

Appendix

Mobility Measurements in *Doped* Organic Semiconductors. We briefly discuss the conventional methods of measuring the mobility in OSCs in order to show why they are not applicable to our doped system. First, measurements of space-charge-limited currents, SCLC,[24,43] in insulators are commonly employed to estimate carrier mobilities. SCLC is the highest current density possible in a single carrier device and is governed only by the device capacitance. Therefore, knowledge of the carrier density is not required to calculate the carrier mobility. Even if the current is not really SCLC, fitting it to the SCLC equation often appears to be viable and it will provide a lower limit to the actual mobility (Figure 7 and discussion).

SCL currents are easily observed in single crystal OSCs and in molecularly doped polymers[16,43] because n_f is so low that it is easily overwhelmed by the density of injected carriers, n_{inj}. However, as n_f increases due to crystal defects, chemical impurities, added dopants, distorted double bonds in a π-conjugated polymer, etc., it becomes ever more difficult to achieve SCLC. The injected charge density under SCLC conditions is[43]

$$n_{inj} = F\epsilon\epsilon_0/qd \qquad \text{(A1)}$$

If we take typical values of $F = 10^3-10^6$ V/cm, $\epsilon = 4$, and $d = 4$ μm, n_{inj} takes on values between $n_{inj} = 5 \times 10^{12}$ and 5×10^{15} cm^{-3}. For comparison, our lowest achievable doping density in the PPEEB films is $n_d \approx 4 \times 10^{16}$ cm^{-3}, which at $F = 10^3$ V/cm corresponds approximately to $n_f \approx 4 \times 10^{13}$ cm^{-3}. To observe pure SCLC, n_{inj} should be $10-100 \times n_f$ at the applied field strength. In other words, even our lowest achievable doping density is 2−3 orders of magnitude too high to observe pure SCLC as shown in Figures 3, 4 and 7 and their discussions. Observation of SCLC normally requires pristine XSCs, not the sort of materials studied for practical organic photovoltaic cells. SCL currents can be easily obscured by n_f in disordered or doped materials, especially at low fields, and may not be observable at all in materials such as conducting polymers where "undoped" materials may have $n_f \approx 10^{15}-10^{17}$ cm^{-3}.[11,58] Unfortunately, SCL currents are easily mistaken for PF-like currents (eqs 3 and 7 and Figure 7).[10] The great advantage of SCL currents, if they are real, is that one can calculate the carrier mobility directly without knowing n_f. The great disadvantage of believing that one is measuring SCL currents when in fact one is measuring PF currents is that changes in n_f are misinterpreted as being changes in μ_f.

Mobility measurements using a field-effect transistor (FET) device geometry are an excellent method for estimating mobility in undoped materials. However, the values obtained depend strongly on the orientation of molecules (or polymer chains) near the substrate (gate electrode) because the conducting channel is localized within a nanometer or two of the gate. Undoped PPEEB films show rather low values of μ_f ($\sim$0.02 cm^2/Vs) in such measurements, apparently because the first monolayer or two on a substrate is oriented parallel to the substrate, that is, almost perpendicular to the bulk orientation (unpublished results). Moreover, FET measurements are not expected to be valid for doped materials because the field induced by the gate electrode effects only the few layers closest to the gate. The conductivity can be "shut off" in the few layers closest to the gate but will remain in the rest of the film; thus the "turn-off" voltage cannot be employed to accurately describe an FET measurement unless the film is only a few monolayers thick.

Time-of-flight (TOF) measurements are one of the least ambiguous methods of estimating charge carrier mobilities.[16] Again, they require undoped or very weakly doped samples because they rely on a large difference between the dark and light currents. High dark currents in doped samples can invaldate the analysis. Unfortunately, the mobility in even undoped PPEEB films cannot be measured by TOF because the orientation of the molecules in the bulk films is such that the conducting axis is parallel to the substrate.[13] TOF, however, measures the mobility perpendicular to the substrate, and thus is of no use in measurements of PPEEB films.

Seebeck and Hall Effect Measurements. There appear to be no viable ways to unambiguously measure μ_f independent of n_f in doped samples except via Hall effect measurements[43] or, in principle, via Seebeck effect measurements.[27,43] We made a serious effort to employ Seebeck (thermopower) measurements to estimate the free electron density in our doped films, using a calibrated measurement system that gives correct results for conventional semiconductors.[54] However, these measurements, at least when interpreted by simple theory,[27,28] led to nonsensical results. We know from conductivity and EPR studies[44] that the carrier density in the undoped PPEEB films is insignificant ($\sim 10^9$ cm^{-3}). Yet when we add, for example, 10^{17} cm^{-3} dopants to the films, the conventional analysis of Seebeck measurements results in a calculated carrier density of $\sim 10^{19}$ cm^{-3} electrons. These experimental results are reproducible but their interpretation is obviously wrong. We conclude that conventional theory does not correctly describe the Seebeck effect in doped, polycrystalline OSCs. Thus, we turned our attention to Hall effect measurements.

In the 1950s, at the dawn of the semiconductor age, Hall effect measurements versus temperature were the method of choice to characterize new semiconductors.[45,46] They provided directly the majority carrier type, the carrier density, and the carrier mobility as a function of temperature. However, Hall effect measurements have not yet been successfully employed to characterize organic semiconductors because of signal-to-noise problems. The relatively low carrier mobility and carrier density of OSC films (i.e., their high resistivity) make Hall effect measurements very difficult.[43] Since our doped films have, by organic standards, both a relatively high mobility and a high free carrier density, we devoted a substantial effort to Hall effect

measurements. Our results at the highest doping densities (0.1−1 mol %) are encouraging but still not definitive. We cannot yet unambiguously separate n_f from μ_f because the reproducibility of the individual parameters is not yet better than a factor of 10. However, the product, $n_f\mu_f$, is reproducible to within ±50%. Since these measurements are performed close to equilibrium ($F \sim 10$ V/cm), we can use the zero field activation energies discussed earlier to obtain an estimate of n_f and therefore μ_f.

To summarize the state of the mobility-measuring art in doped organic thin films: we can at present accurately measure only the $n_f\,\mu_f$ product, unless for example, n_f can be estimated via a known doping density, n_d, or if μ_f is known from independent experiments. This unfortunate state of affairs is not restricted to purposely doped OSCs; it applies also to adventitiously doped films such as conducting polymers.[11]

Acknowledgment. This work was funded by the U.S. Department of Energy, Office of Science, Basic Energy Sciences (S.C. and B.A.G.), and by the Office of Energy Efficiency and Renewable Energy (P.S.), under Contract No. DE-AC36-99GO10337.

References and Notes

(1) Law, K.-Y. *Chem. Rev.* **1993**, *93*, 449.
(2) Special Issue on Organic Electronics; Jenehke, S., Ed. *Chem. Mater.* **2004**, *16*, 23.
(3) Organic-Based Photovoltaics. *MRS Bull.* **2005**, *30*, 1.
(4) Gregg, B. A.; Hanna, M. C. *J. Appl. Phys.* **2003**, *93*, 3605.
(5) Gregg, B. A. *J. Phys. Chem. B* **2003**, *107*, 4688.
(6) Forrest, S. R. *Chem. Rev.* **1997**, *97*, 1793.
(7) Blom, P. W. M.; Vissenberg, M. C. J. M. *Mater. Sci. Eng.* **2000**, *27*, 53.
(8) Heeger, A. J. *J. Phys. Chem. B* **2001**, *105*, 8475.
(9) Gregg, B. A.; Chen, S.-G.; Branz, H. M. *Appl. Phys. Lett.* **2004**, *84*, 1707.
(10) Gregg, B. A. Coulomb Forces in Excitonic Solar Cells. In *Organic Photovoltaics*; Sun, S. S., Sariciftci, N. S., Eds.; Marcell Dekker: New York, 2005; p 139.
(11) Gregg, B. A.; Chen, S.-G.; Cormier, R. A. *Chem. Mater.* **2004**, *16*, 4586.
(12) Gregg, B. A. *J. Phys. Chem. B* **2004**, *108*, 17285−17289.
(13) Liu, S.-G.; Sui, G.; Cormier, R. A.; Leblanc, R. M.; Gregg, B. A. *J. Phys. Chem. B* **2002**, *106*, 1307.
(14) Gregg, B. A.; Cormier, R. A. *J. Am. Chem. Soc.* **2001**, *123*, 7959.
(15) Borsenberger, P. M.; Fitzgerald, J. J. *J. Phys. Chem.* **1993**, *97*, 4815.
(16) Van der Auweraer, M.; De Schryver, F. C.; Borsenberger, P. M.; Bässler, H. *Adv. Mater.* **1994**, *6*, 199.
(17) Bässler, H. *Phys. Status Solidi* **1993**, *175*, 15.
(18) Arkhipov, V. I.; Heremans, P.; Emilianova, E. V.; Adriaenssens, G. J.; Bässler, H. *Appl. Phys. Lett.* **2003**, *82*, 3245.
(19) Rakhmanova, S. V.; Conwell, E. M. *Appl. Phys. Lett.* **2000**, *76*, 3822.
(20) Novikov, S. V.; Dunlap, D. H.; Kenkre, V. M.; Parris, P. E.; Vannikov, A. V. *Phys. Rev. Lett.* **1998**, *81*, 4472.
(21) Gartstein, Y. N.; Conwell, E. M. *Phys. Rev. B.* **1995**, *51*, 6947.
(22) Bozano, L.; Carter, S. A.; Scott, J. C.; Malliaras, G. G.; Brock, P. J. *Appl. Phys. Lett.* **1999**, *74*, 1132.
(23) Malliaras, G. G.; Salem, J. R.; Brock, P. J.; Scott, C. *Phys. Rev. B* **1998**, *58*, R13411.
(24) Tanase, C.; Meijer, E. J.; Blom, P. W. M.; de Leeuw, D. M. *Phys. Rev. Lett.* **2003**, *91*, 216601.
(25) Blom, P. W. M.; Tanase, C.; de Leeuw, D. M.; Coehoorn, R. *Appl. Phys. Lett.* **2005**, *86*, 092105.
(26) Tanase, C.; Blom, P. W. M.; de Leeuw, D. M. *Phys. Rev. B* **2004**, *70*, 193202.
(27) Pfeiffer, M.; Beyer, A.; Fritz, T.; Leo, K. *Appl. Phys. Lett.* **1998**, *73*, 3202.
(28) Pfeiffer, M.; Beyer, A.; Plönnigs, B.; Nollau, A.; Fritz, T.; Leo, K.; Schlettwein, D.; Hiller, S.; Wörhle, D. *Sol. Energy Mater. Sol. Cells* **2000**, *63*, 83.
(29) Maennig, B.; Pfeiffer, M.; Nollau, A.; Zhou, X.; Leo, K.; Simon, P. *Phys. Rev. B* **2001**, *64*, 195208.
(30) Werner, A. G.; Li, F.; Harada, K.; Pfeiffer, M.; Fritz, T.; Leo, K. *Appl. Phys. Lett.* **2003**, *82*, 4495.
(31) Lonergan, M. C.; Cheng, C. H.; Langsdorf, B. L.; Zhou, X. *J. Am. Chem. Soc.* **2002**, *124*, 690.
(32) Leempoel, P.; Fan, F.-R. F.; Bard, A. J. *J. Phys. Chem.* **1983**, *87*, 2948.
(33) Kearns, D. R.; Tollin, G.; Calvin, M. *J. Chem. Phys.* **1960**, *32*, 1020.
(34) Avakian, P.; Merrifield, R. E. *Mol. Cryst. Liq. Cryst.* **1968**, *5*, 37.
(35) Davydov, A. S. *Theory of Molecular Excitons*; Plenum: New York, 1971.
(36) Gregg, B. A. *Appl. Phys. Lett.* **1995**, *67*, 1271.
(37) Haugeneder, A.; Neges, M.; Kallinger, C.; Spirkl, W.; Lemmer, U.; Feldman, J.; Scherf, U.; Harth, E.; Gügel, A.; Müllen, K. *Phys. Rev. B* **1999**, *59*, 15346.
(38) Kenkre, V. M.; Wong, Y. M. *Phys. Rev. B* **1980**, *22*, 5716.
(39) Markovitsi, D.; Lecuyer, I.; Simon, J. *J. Phys. Chem.* **1991**, *95*, 3620.
(40) Powell, R. C.; Soos, Z. G. *J. Lumin.* **1975**, *11*, 1.
(41) Kenkre, V. M.; Parris, P. E.; Schmidt, D. *Phys. Rev. B* **1985**, *32*, 4946.
(42) Gregg, B. A.; Sprague, J.; Peterson, M. *J. Phys. Chem. B* **1997**, *101*, 5362.
(43) Pope, M.; Swenberg, C. E. *Electronic Processes in Organic Crystals and Polymers*, 2nd ed.; Oxford University Press: New York, 1999.
(44) Chen, S.-G.; Branz, H. M.; Eaton, S. S.; Taylor, P. C.; Cormier, R. A.; Gregg, B. A. *J. Phys. Chem. B* **2004**, *108*, 17329.
(45) Debye, P. P.; Conwell, E. M. *Phys. Rev.* **1954**, *93*, 693.
(46) Pearson, G. L.; Bardeen, J. *Phys. Rev.* **1949**, *75*, 865.
(47) Smith, R. A. *Semiconductors*; Cambridge University Press: Cambridge, 1978.
(48) Frenkel, J. *Phys. Rev.* **1938**, *54*, 647.
(49) Katz, H. E.; Bau, Z. *J. Phys. Chem. B* **2000**, *104*, 671.
(50) In amorphous π-conjugated polymers there is a coupling between *effective* mobility and *total* carrier density caused by filling of traps with increasing n.[25,26] However, this does not affect the *free carrier* values, n_f and μ_f, employed in our treatment.
(51) Blom, P. W. M.; de Jong, M. J. M.; van Munster, M. G. *Phys. Rev. B* **1997**, *55*, R656.
(52) Cormier, R., A.; Gregg, B. A. *J. Phys. Chem.* **1997**, *101*, 11004.
(53) Cormier, R. A.; Gregg, B. A. *Chem. Mater.* **1998**, *10*, 1309.
(54) Young, D. L.; Coutts, T. J.; Kaydanov, V. I. *Rev. Sci. Instrum.* **2000**, *71*, 462.
(55) Reynaert, J.; Arkhipov, V. I.; Borghs, G.; Heremans, P. *Appl. Phys. Lett.* **2004**, *85*, 603.
(56) Borsenberger, P. M.; Pautmeier, L.; Bässler, H. *J. Chem. Phys.* **1991**, *94*, 5447.
(57) Branz, H. M.; Gregg, B. A. *Mater. Res. Soc. Proc.* **2002**, *725*, 205.
(58) Jain, S. C.; Geens, W.; Mehra, A.; Kumar, V.; Aernouts, T.; Poortmans, J.; Mertens, R.; Willander, M. *J. Appl. Phys.* **2001**, *89*, 3804.
(59) Smith, D. L. *Synth. Met.* **2004**, *141*, 122−128.